

Self-sustained Films of Cellulose/Graphite Composites: Mechanical and Water Vapor Barrier Properties

Cibele Carneiro Pessan^a , Juliana S. Bernardes^b, Sílvia H. P. Bettini^{a,c}, Edson R. Leite^{a,b,d,*}

^aUniversidade Federal de São Carlos (UFSCar), Programa de Pós-Graduação em Ciência e Engenharia de Materiais (PPG-CEM), Rodovia Washington Luiz, Km 235, 13.565-905, São Carlos, SP, Brasil.

^bCentro Nacional de Pesquisa em Energia e Materiais (CNPEM), Laboratório Nacional de Nanotecnologia (LNNano), Rua Giuseppe Máximo Scolfaro, 10.000, 13.083-100, Campinas, SP, Brasil.

^cUniversidade Federal de São Carlos (UFSCar), Departamento de Engenharia de Materiais (DEMa), Rodovia Washington Luiz, Km 235, 13.565-905, São Carlos, SP, Brasil.

^dUniversidade Federal de São Carlos (UFSCar), Departamento de Química (DQ), Rodovia Washington Luiz, Km 235, 13.565-905, São Carlos, SP, Brasil.

Received: January 14, 2023; Revised: March 29, 2023; Accepted: May 10, 2023

Cellulosic materials have several applications, from rheological modifiers to structural reinforcement and packaging components. Using cellulosic materials may also contribute to environmental sustainability because it can be sourced from agricultural byproducts. In this work, self-sustained composite films were produced by the casting of TEMPO-oxidized cellulose nanofibers/graphite composite dispersions. Oscillatory rheology and tensile strength tests showed that the presence of graphite did not significantly contribute to the enhancement of neither the rheological nor mechanical properties of the dispersions and films. Morphological analysis showed that particle segregation and setting occurred during film casting, resulting in particle concentration gradient along the thickness of the film. These results could indicate the low exfoliation efficiency of the microfluidization process and, therefore, justify why the graphite did not act as a reinforcement of the cellulose matrix. However, the graphite particles contributed to a higher barrier to water vapor permeation of the cellulosic films.

Keywords: Nanocellulose, Graphite, Mechanical properties, Rheology, WVTR.

1. Introduction

Cellulosic materials can be applied in the pharmaceutical, food, automotive and packaging industries. They are an interesting option as mechanical reinforcement due to their excellent mechanical properties allied to low density (specific strength) and compatibilization possibilities. The hydroxyl chemical groups available at the surface of the cellulose fibers allow for several routes of chemical functionalization, which can improve their compatibility with other materials – both organic and inorganic. These hydroxyl groups are also responsible for forming structured networks when cellulose is dispersed in water, capable of stabilizing dispersions of many different components. Besides the attractive mechanical and chemical properties, cellulosic materials also present environmental benefits, since they can be sourced from renewable agricultural byproducts, contributing to the circular economy strategy¹.

Celluloses in the nanoscale range are cellulose nanocrystals (CNCs) and cellulose nanofibers (CNFs). CNCs are produced by acid hydrolysis, that dissolves the amorphous regions in the cellulose structure, yielding highly crystalline whisker-like nanoparticles (5-10 nm wide and up to 500 nm long). On the other hand, CNFs are isolated by mechanical routes, often combined with chemical processes, and present alternating crystalline and amorphous regions (5-10 nm wide and several micrometers long)^{2,3}.

Microfluidization is a high-pressure homogenization process in which a liquid dispersion is subjected to high shear and impact forces. It is useful for nanoemulsion production, particle deagglomeration and size reduction, cell disruption, and physical encapsulation. Like other mechanical processes, it can fibrillate hierarchical cellulose fibers, exposing the singular fibrils, yielding low-concentration CNF dispersions. The rheological properties of the resulting dispersion strongly depend on the fibril length, which shortens with prolonged exposure to mechanical stress^{1,4}.

Microfluidization can also be used to delaminate layered materials into 2D particles. It has been shown that graphite flakes dispersed in deionized water (in the presence of a dispersion agent) were cycled through a microfluidizer to produce nanolayers. After achieving nano graphite particles (width between 4 and 70 nm), including few-layer graphene (FLG) (<4 nm in thickness), cellulose derivatives can be used to stabilize the dispersions and prevent the decantation of solid particles^{5,6}.

Alternatively, researchers have succeeded in exfoliating graphite flakes in cellulose alkaline solution or in the presence of CNCs and CNFs. The amphiphilic nature of cellulose is responsible for the graphite exfoliation, dispersing single or multiple sheets of graphite in water⁷⁻⁹.

The exfoliation and intercalation of graphite particles by cellulose fibers allow for the production of composite films

*e-mail: edson.leite@lnnano.cnpem.br

with good particle dispersion and distribution, which is essential for the improvement of the material's mechanical properties. Besides the mechanical reinforcement of cellulose films, graphite particles may add to other functionalities. The platelet shape of the nano graphite and few layer graphene particles makes the material a good candidate for gas barrier improvement¹⁰⁻¹². On different applications, the electrical and thermal conductivity of graphite can be exploited to produce conductive paper and inks, where cellulose acts as support medium or binder^{6,10,13,14}.

This work aimed to produce a hybrid composite material by casting dispersions that were processed by microfluidization. Fibrillation of TEMPO-oxidized cellulose fibers, exfoliation of graphite flakes, and homogenization in water occurred simultaneously. This method is simple and promising to produce composite films with high graphite concentration and improved barrier, electrical, and thermal properties. The materials were characterized by oscillatory rheology, electron microscopy, tensile test, and water vapor permeation test.

2. Experimental

2.1. Materials

The sugarcane bagasse was sourced by Brazilian Biorenewables National Laboratory from Brazilian Centre for Research in Energy and Materials (LNBR – CNPEM, Campinas – SP – Brazil). Chemical reagents 2,2,6,6-Tetramethylpiperidine 1-oxyl (TEMPO) (98%), NaClO (Reagent grade 10-15% available chlorine solution), and graphite flakes were acquired from Sigma-Aldrich/Merck and NaCl (P.A. A.C.S. reagent powder), NaOH (P.A. pellets), NaBr (P.A. A.C.S. reagent powder), and HCl (P.A. A.C.S. reagent 37% solution) were acquired from Synth.

2.2. Cellulose organosolv extraction

As described by Oliveira *et al.*¹⁵, sugarcane bagasse and equal-part mixture of water and ethanol (100 g: 1 L) were placed in a Parr reactor and heated to 190 °C and 30 bar for 120 minutes. Then, the pulp was agitated in a disintegrator in presence of NaOH solution (1% w/w), then sieved and washed until neutral pH was obtained.

2.3. Cellulose pulp bleaching

The bleaching reacting was done as described by Teixeira *et al.*¹⁶. The cellulose pulp and a mixture of NaOH solution (500 mL, 5% m/v) were heated to 70 °C, and under continuous agitation, H₂O₂ solution (500 mL, 24% v/v) was dripped over the mixture. Following, the dispersion was sieved and washed until neutral pH was obtained.

2.4. TEMPO-mediated-oxidation

The dispersion of bleached cellulose was oxidized according to the methodology described by Saito *et al.*¹⁷. The TEMPO-mediated-oxidation occurred in the presence of NaBr and NaClO, at a controlled pH of 10 for 130 minutes. The dispersion was washed until neutral pH dispersion was obtained.

2.5. Microfluidization

A mixture of graphite flakes and TEMPO-oxidized-cellulose (TOC) dispersion was mechanically treated with

the MP110 Microfluidizer from Microfluidics, equipped with H30Z and G10Z interaction chambers. The dispersions were cycled through the equipment 25 times, under process pressure ranging from 25,000 to 30.000 psi. The TOC concentration was 1 wt% solids content, and the graphite flakes were added at 1 wt%, 5 wt% and 50 wt%, in proportion to the cellulose present in the dispersion.

2.6. Cellulose film casting

To produce self-sustained films, the TOC-graphite dispersions were placed on glass Petri dishes and were oven dried at 45 °C overnight. After cooling, the films were manually removed from the bottom of the Petri dishes.

2.7. Rheological characterization of composite dispersions

The dispersions' rheological behavior was analyzed by oscillatory rheology. Oscillatory strain sweep was done at 1 rad.s⁻¹ frequency and strain ranging from 10⁻¹ to 10^{1%}; Oscillatory frequency sweep was done at 1% strain and frequency ranging from 10⁻² to 10² rad.s⁻¹. The equipment used was ARES rheometer from TA Instruments, in concentric cylinder geometry (bob with 31.9 and 25 mm length and diameter, respectively, and cup of 27 mm diameter). Measurements were done in triplicates, at room temperature (23 °C), with rested samples (at least 8 hours without prior manipulation).

2.8. Morphological characterization

The dispersions were analyzed by Cryogenic Transmission Electron Microscopy (Cryo-TEM), on JEM 1400 Plus microscope from JEOL (120 kV). The surface and cross-section of the self-standing films were analyzed by Scanning Electron Microscopy (SEM), on Scios 2 equipment from Thermo Fischer Scientific, under vacuum, 50 pA beam and 1Kv voltage.

2.9. Water vapor transmission rate test

The water vapor transmission rate (WVTR) test was performed based on ASTM testing standards D1653¹⁸, Test method A - dry cup method. Pre-conditioned films (24h at 23 °C and 50% RH) were placed on an aluminum mask with a 3 mm diameter test area and sealed onto glass cups containing dried (24 h at 200 °C) calcium chloride. The testing cups were placed in a controlled environment chamber, at 19 ± 5 °C and 75% relative humidity, controlled by saturated sodium chloride salt (NaCl) solution, according to ASTM testing standard E104¹⁹. The weight of each testing cup was measured every 24 hours for at least 4 days. WVTR was calculated from the average of at least 3 curve slopes, and the permeability of the materials was calculated as follows:

$$WVT = \frac{\Delta G}{\Delta t} \times \frac{1}{A} \quad (1)$$

$$Permeability = \frac{WVT \times T}{S \times (R_1 - R_2)} \quad (2)$$

Where:

- $\Delta G / \Delta t$ is the slope of gained mass curve;
- A is the exposed area of the film;
- T is the thickness of the film;
- S is the saturation vapor pressure at the test temperature;
- R₁ is the relative humidity at the vapor source;
- R₂ is the relative humidity at the vapor sink.

2.10. Tensile strength test

The tensile test was based on ASTM testing standard D882²⁰. Rectangular sections of films were cut from the casted films 10 mm x 50 mm. The equipment used was universal testing machine DL 2000 from EMIC, with a 5N load cell, initial gauge length of 40 mm and testing speed of 60 mm/min.

3. Results and Discussion

Initially, sugarcane bagasse was chemically treated through organosolv pulping (for cellulose extraction), bleaching, and oxidation in the presence of TEMPO. Then, the oxidized pulp was mechanically treated with the microfluidizer to produce cellulosic dispersions. The dispersions produced were of pristine TOC and composites with 1, 5 and 50 wt% of graphite in proportion to the cellulose content. Figure 1 shows the evolution of the cellulosic pulp's appearance throughout the sequence of chemical and mechanical procedures.

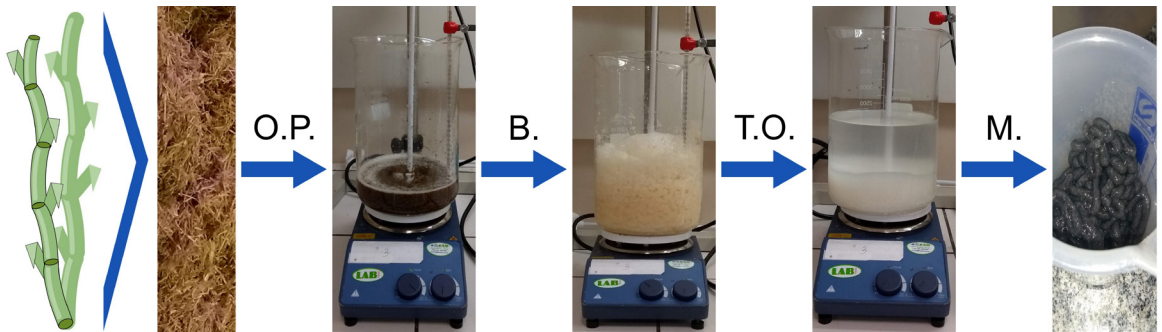


Figure 1. Sequential appearance of sugarcane bagasse after organosolv pulping (O.P.), pulp after bleaching (B.) and after TEMPO-mediated-oxidation (T.O.), and composite dispersion produced after microfluidization with graphite flakes (M.).

3.1. Rheological characterization

The rheological tests were performed on the cellulosic dispersions (reference cellulose dispersion and 1, 5 and 50 wt% composite dispersions). Oscillatory strain sweep was used to determine the viscoelastic region of the dispersions. As seen in Figure 2A, the critical strain value (γ_c) decreased with the addition of graphite, indicating that the graphite particles do not contribute to the stabilization of the suspension. The addition of small amounts of graphite decreased γ_c from 3.5% to values above 2%. However, the dispersion with 50 wt% of graphite presented γ_c below 1%.

The oscillatory frequency sweep curves are presented in Figures 2B and 2C. It is noticeable that the storage modulus and viscosity decrease with the addition of small amounts of graphite (1 and 5 wt%), indicating that the graphite particles act as a component that favors flow. The 50 wt% sample showed an increase in viscosity, but this should be related to the higher solids content of this dispersion and not a change in the flow facilitating behavior.

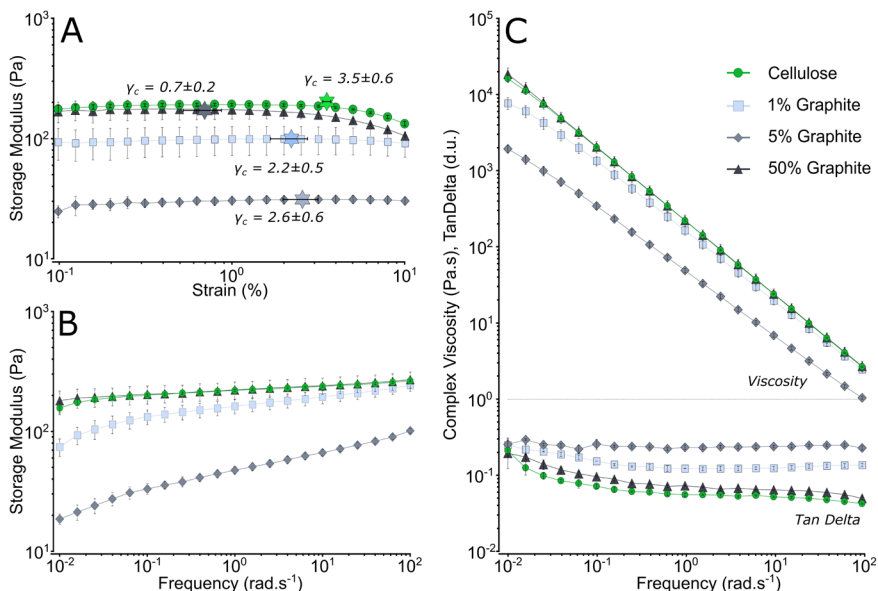


Figure 2. (A) Oscillatory strain sweep curve: storage modulus; Frequency sweep curves: (B) storage modulus and (C) complex viscosity and tan delta ($\tan(\delta)$).

Furthermore, all samples presented $\tan(\delta)$ values below 1, which indicates gel-like rheological behavior. Another feature of gel-like rheological behavior is when the storage modulus is independent of the frequency. The composition with 1 wt% graphite content diverged slightly from the pristine cellulose dispersion behavior, while the 5 wt% sample presented an even higher dependency on frequency. This trend suggests that the addition of graphite alters the connectivity of CNFs network, changing the viscoelastic response. As observed by Cryo-TEM, shown in Figure 3, graphite sheets fit between the cellulose nanofibers. The nanoparticles remain electrostatically stabilized in the dispersion due to the interaction of the Na^+ counter-ions (from cellulose surface carboxylate groups) with the graphite sp^2 lattice¹⁴.

In contrast, the storage modulus curve for the 50 wt% dispersion follows the rheological behavior of the pristine cellulose dispersion. As mentioned regarding the increase in viscosity, this behavior should also be related to the higher solids content of this dispersion rather than a change in the effects of graphite content over the rheological behavior.

3.2. Film morphology

The appearance of the films resulting from the casting process is presented in Figure 4. Whereas the cellulose film is transparent and presents no coloration, the 1 wt% graphite composite film presents a gray hue while remaining translucent. The 5 wt% composite, on the other hand, loses all transparency and exhibits a graphite-like sheen. The 50 wt% composite film is also opaque but presents different appearances for each side of the film: the top surface exhibits a glossy shine, while the bottom surface (the side in contact with the glass during casting) has a graphite-like metallic appearance.

The composite films remain flexible but are more delicate to handle regarding tear resistance than the pristine cellulose film. Due to this characteristic, the casting method could not produce large film samples with 50 wt% of graphite, as it would tear in random shapes during its removal from the Petri dish.

To investigate the morphology of the composites, SEM images were taken of the surface and cross-section of the films, as shown in Figure 5.

The samples with 1 and 5 wt% of graphite content are homogeneous along the film's thickness, not being possible to identify differences between the film sides. However, in the 50 wt% sample, a higher concentration of graphite particles at the bottom side of the film can be visualized. This is also clear by comparing Figure 5D and 5E. Although there are some graphite particles visible in the top side view, the bottom side is completely covered by graphite.

3.3. Mechanical properties

The mechanical properties of the films were measured by tensile test. Since it was not possible to produce test specimens of the 50 wt% graphite composite sample, only the samples up to 5 wt% of graphite content were tested. The tensile test results are shown in Figure 6.

The common expectation for adding of inorganic particles in polymers is that the elastic modulus and tensile strength would rise to the detriment of the elongation – unless there is good compatibility between matrix and fillers. However, the results show quite the opposite. The film's stiffness and

tensile resistance decreased by approximately 14% and 22%, respectively, with the addition of 5 wt% graphite, with no significant change in the elongation at break value. The reduction of film stiffness also suggests a loss of connectivity of the nanofiber network with the addition of graphite.

Similar reinforcing behavior for cellulose and graphite/few-layer graphene composites have been reported in the literature^{8,10,21}. Even though it was possible to produce flexible cellulose composite films with high particle content, the elastic modulus and tensile strength decreased continuously with further particle incorporation, after an initial increase for lowly concentrated compositions (below 2 wt%). At the same time, the addition of particles had no significant effect on the elongation at break, except for the extremely high concentration of graphite (90%), where the elongation at break dropped substantially²¹. Yet, an important distinction can be pointed out: even the most concentrated composition did not exhibit particle segregation and the distribution along the film thickness was homogeneous.

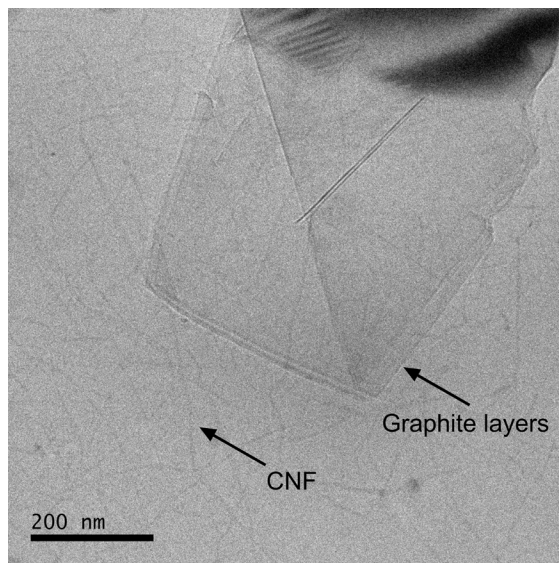


Figure 3. Cryogenic TEM image of cellulose-graphite dispersion.

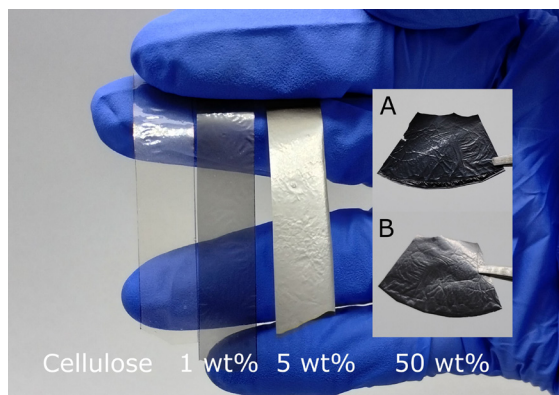


Figure 4. Cast film samples; (A) top side and (B) bottom side view of 50 wt% graphite composite film.

Contrary to what happened in this work, there was no segregation of graphite nanoparticles at one side of the film.

These results indicate that the limit for the graphite particles addition into the cellulose matrix also depends on the film production process. The films cited in this work, produced by Malho et al.⁸ and Li et al.²¹, probably did not exhibit segregation because of the process chosen for film fabrication, i.e., vacuum filtration followed by oven drying. Because the samples studied in this work were produced by casting, the time to produce the film was much longer than the stability of the 50 wt% composite dispersion. Thus, the 10-hour process resulted in enough time for the phases to separate and for graphite particles to sediment at the bottom of the film.

Another aspect regarding the film's morphology and stability that could be considered is the compatibility between particle and matrix and how much of the graphite particles the cellulose dispersion is able to suspend. As presented previously in Figure 3, the cellulose nanofibers form a three-dimensional network in which the graphite nanoparticles are dispersed. The stabilization of the dispersion is due to the interactions between the surface charge of the cellulose fibers and the sp^2 lattice of graphite structure. The more negatively charged the cellulose surface is, the higher graphite content can be stabilized¹⁴.

Therefore, the particle segregation shown by the 50 wt% cellulose/graphite composite could be attributed to the combination of two factors: low exfoliation efficiency and insufficient CNF surface charge. In contrast to the 1 and 5 wt% graphite compositions, the 50 wt% composite could present lower delamination yield, consequently there would be less graphitic surface area available for interaction with the CNFs. The same reasoning can be applied to the CNF surface charge: a more negatively charged TOC would be able to stabilize higher graphite content. Therefore, as a consequence of a combination of both factors, the excess graphite content settled during casting process.

3.4. Water vapor barrier properties

The cellulosic films were tested for resistance to water vapor permeation. The water vapor transmission of a sample depends on many variables: the relative humidity from the water source, the temperature during testing, the area available for the permeation to occur, and the sample's thickness. The water vapor permeability, however, takes these variables into account during calculations, meaning that this property can be compared across samples that present different dimensions or even testing conditions. Table 1 presents the results of the WVTR test, as required by the ASTM D1653 standard, and Figure 7 presents a box plot chart for the water vapor permeability values for each sample.

The results show that the barrier to the permeation of water vapor increases with the addition of graphite. The sample with 50 wt% graphite content presented half the permeability value of the pristine cellulose film. This value is at the threshold between poor and low water vapor barrier category (from 1000 to 3000 $g \cdot \mu m \cdot m^{-2} \cdot 24 h^{-1} \cdot kPa^{-1}$), which includes materials like PA and PLA¹¹.

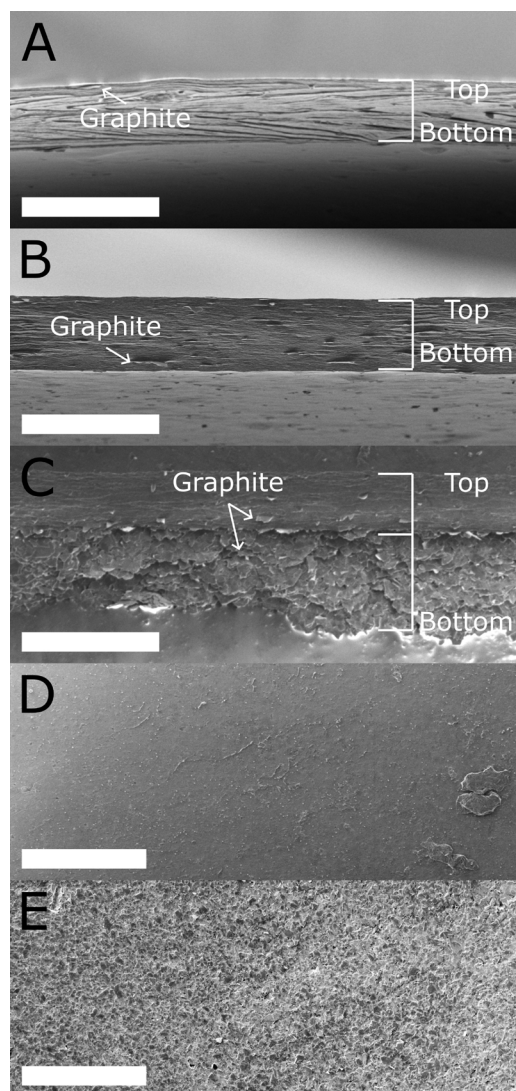


Figure 5. Secondary electrons SEM images of film samples. Cross-section images of (A) 1 wt% graphite composite, (B) 5 wt% graphite composite, (C) 50 wt% graphite composite (scale bar equals 20 μm); Surface images of (D) top and (E) bottom side of 50 wt% graphite composite film (scale bar equals 50 μm).

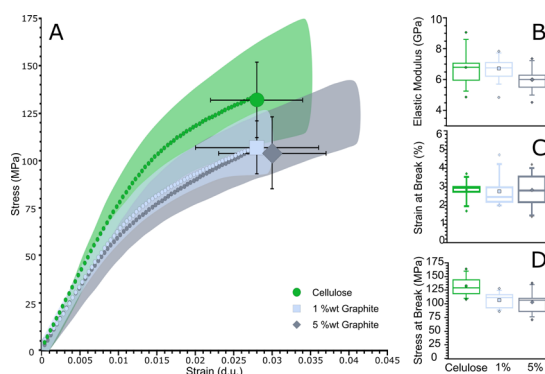
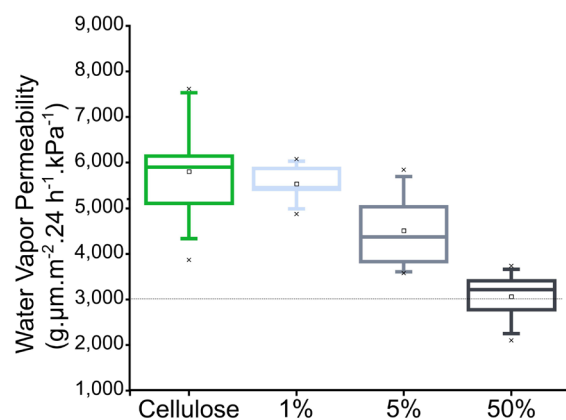


Figure 6. (A) Representative stress vs strain curves and box plots charts for (B) Elastic modulus, (C) Tensile Strength and (D) Elongation at break of films produced by casting.

Table 1. Water vapor permeation test results for cellulosic films produced by casting.

Property	Cellulose	1 wt% graphite	5 wt% graphite	50 wt% graphite
Thickness (μm)	12.2 ± 0.3	12.6 ± 2.0	14.4 ± 1.3	6.7 ± 1.6
Water Vapor Transmission (WVT) (grams of water/ m^2 , 24 hours)	846 ± 112	744 ± 78	525 ± 109	769 ± 167
Water Vapor Permeance (WVP in perm unit) ($\text{grains}^*/\text{ft}^2 \cdot 1 \text{ h.inHg}$)	103 ± 15	89 ± 8	63 ± 16	92 ± 19
Water Vapor Permeance (WVP in metric perm unit) $\text{g}/\text{m}^2 \cdot 24 \text{ h.mmHg}$)	68 ± 10	59 ± 5	42 ± 8	61 ± 12
Water Vapor Permeability ($\text{g} \cdot \mu\text{m} / \text{m}^2 \cdot 24 \text{ h.kPa}$)	$5,805 \pm 1,061$	$5,541 \pm 465$	$4,512 \pm 887$	$3,063 \pm 591$

*1 g equals 15.43 grains

**Figure 7.** Water vapor permeability boxplot chart.

The water vapor permeability of cellulosic materials is found between 2,800 to 28,000 $\text{g} \cdot \mu\text{m} \cdot \text{m}^{-2} \cdot 24 \text{ h}^{-1} \cdot \text{kPa}^{-1}$ and depends on the film's production method, surface treatments and addition of inorganic particles. This improvement is due to the compact layer of graphite formed at the bottom of the film during the casting process. The barrier property can be further improved by pressing the films, which reduces its overall porosity. Both the presence of platelet particles and pore reduction decrease the mobility of water molecules across the film^{11,12}

4. Conclusions

In this work, self-sustained films of cellulose matrix with graphite particles were successfully prepared by the simultaneous exfoliation of graphite flakes and fibrillation of TOC during the microfluidization process. Rheological analysis showed that the presence of graphite particles (from 1 to 5 wt%) altered the rheological behavior of the cellulose dispersions, diverging from the gel-like behavior, due to the reduction of CNF network connectivity.

Morphological analysis showed that the films prepared with high graphite concentration (50 wt%) presented separation of layered particles from the dispersion during the casting process and segregation occurred. Phase separation indicates that this composition presented low yield of graphite delamination and excess of graphite content in comparison to the available counter ions at the surface of the cellulose fibers. Even though the casted films remained flexible, the tensile test results showed that there was no enhancement of the mechanical properties of the composite films.

The presence of graphite particles (from 1 to 5 wt%) altered the mechanical behavior of the cellulose dispersions and films due to the reduction of CNF network connectivity.

On the other hand, the water vapor transmission test showed that the platelet particles improved the barrier to water vapor permeation through the films. Hence, it was possible to produce cellulosic films with better gas barrier properties without compromising their mechanical performance.

5. Acknowledgments

This study received grant no. 140459/2018-9 from the National Council for Scientific and Technological Development (CNPq).

This study was financed in part by the Coordenação de Aperfeiçoamento de Pessoal de Nível Superior - Brasil (CAPES) - Finance Code 001.

This study was also financed in part by the São Paulo Research Foundation (FAPESP), CEPID 2013/07296-2.

This research used facilities of the Brazilian Nanotechnology National Laboratory (LNNano), part of the Brazilian Centre for Research in Energy and Materials (CNPEM), a private non-profit organization under the supervision of the Brazilian Ministry for Science, Technology, and Innovations (MCTI). The microscopy facilities' staff is acknowledged for the assistance during the experiments of SEM and Cryo-TEM.

6. References

1. Czaikoski A, Cunha RL, Menegalli FC. Rheological behavior of cellulose nanofibers from cassava peel obtained by combination of chemical and physical processes. *Carbohydr Polym.* 2020;248:116744. <http://dx.doi.org/10.1016/j.carbpol.2020.116744>.
2. Habibi Y, Lucia LA, Rojas OJ. Cellulose nanocrystals: chemistry, self-assembly, and applications. *Chem Rev.* 2010;110(6):3479-500. <http://dx.doi.org/10.1021/cr900339w>.
3. Moon RJ, Martini A, Nairn J, Simonsen J, Youngblood J. Cellulose nanomaterials review: Structure, properties and nanocomposites. *Chem Soc Rev.* 2011;40(7):3941-94. <http://dx.doi.org/10.1039/c0cs00108b>.
4. Pessan CC, da Silva Bernardes J, Bettini SHP, Leite ER. Oxidized cellulose nanofibers from sugarcane bagasse obtained by microfluidization: morphology and rheological behavior. *Carbohydr Polym.* 2022;304:120505. <http://dx.doi.org/10.1016/j.carbpol.2022.120505>.
5. Karagiannidis PG, Hodge SA, Lombardi L, Tomarchio F, Decorde N, Milana S, et al. Microfluidization of graphite and formulation of graphene-based conductive inks. *ACS Nano.* 2017;11(3):2742-55. <http://dx.doi.org/10.1021/acsnano.6b07735>.
6. Osong SH, Dahlström C, Forsberg S, Andres B, Engstrand P, Norgren S, et al. Nanofibrillated cellulose/nanographite composite films. *Cellulose.* 2016;23(4):2487-500. <http://dx.doi.org/10.1007/s10570-016-0990-2>.

7. Ferreira ES, da Silva DS, Burgo TAL, Batista BC, Galembeck F. Graphite exfoliation in cellulose solutions. *Nanoscale*. 2017;9(29):10219-26. <http://dx.doi.org/10.1039/C7NR02365K>.
8. Malho JM, Laaksonen P, Walther A, Ikkala O, Linder MB. Facile method for stiff, tough, and strong nanocomposites by direct exfoliation of multilayered graphene into native nanocellulose matrix. *Biomacromolecules*. 2012;13(4):1093-9. <http://dx.doi.org/10.1021/bm2018189>.
9. Carrasco PM, Montes S, García I, Borghei M, Jiang H, Odriozola I, et al. High-concentration aqueous dispersions of graphene produced by exfoliation of graphite using cellulose nanocrystals. *Carbon*. 2014;70:157-63. <http://dx.doi.org/10.1016/j.carbon.2013.12.086>.
10. Li B, Zhong WH. Review on polymer/graphite nanoplatelet nanocomposites. *J Mater Sci*. 2011;46(17):5595-614. <http://dx.doi.org/10.1007/s10853-011-5572-y>.
11. Wang J, Gardner DJ, Stark NM, Bousfield DW, Tajvidi M, Cai Z. Moisture and oxygen barrier properties of cellulose nanomaterial-based films. *ACS Sustain Chem& Eng*. 2018;6(1):49-70. <http://dx.doi.org/10.1021/acssuschemeng.7b03523>.
12. Österberg M, Vartiainen J, Lucenius J, Hippi U, Seppälä J, Serimaa R, et al. A fast method to produce strong NFC films as a platform for barrier and functional materials. *ACS Appl Mater Interfaces*. 2013;5(11):4640-7. <http://dx.doi.org/10.1021/am401046x>.
13. Jabbour L, Gerbaldi C, Chaussy D, Zeno E, Bodoardo S, Beneventi D. Microfibrillated cellulose-graphite nanocomposites for highly flexible paper-like Li-ion battery electrodes. *J Mater Chem*. 2010;20(35):7344-7. <http://dx.doi.org/10.1039/c0jm01219j>.
14. Hajian A, Lindström SB, Pettersson T, Hamed MM, Wågberg L. Understanding the dispersive action of nanocellulose for carbon nanomaterials. *Nano Lett*. 2017;17(3):1439-47. <http://dx.doi.org/10.1021/acs.nanolett.6b04405>.
15. Oliveira FB, Bras J, Pimenta MTB, Curvelo AAS, Belgacem MN. Production of cellulose nanocrystals from sugarcane bagasse fibers and pith. *Ind Crops Prod*. 2016;93:48-57. <http://dx.doi.org/10.1016/j.indcrop.2016.04.064>.
16. Teixeira EM, Bondancia TJ, Teodoro KBR, Corrêa AC, Marconcini JM, Mattoso LHC. Sugarcane bagasse whiskers: extraction and characterizations. *Ind Crops Prod*. 2011;33(1):63-6. <http://dx.doi.org/10.1016/j.indcrop.2010.08.009>.
17. Saito T, Kimura S, Nishiyama Y, Isogai A. Cellulose nanofibers prepared by TEMPO-mediated oxidation of native cellulose. *Biomacromolecules*. 2007;8(8):2485-91. <http://dx.doi.org/10.1021/bm0703970>.
18. ASTM: American Society for Testing and Materials. ASTM D1653: standard test methods for water vapor transmission of organic coating films. (Reapproved 2021). West Conshohocken: ASTM; 2013. <http://dx.doi.org/10.1520/D1653-13R21>.
19. ASTM: American Society for Testing and Materials. ASTM E104: standard practice for maintaining constant relative humidity by means of aqueous solutions. (Reapproved 2012). West Conshohocken: ASTM; 2014. <http://dx.doi.org/10.1520/E0104-02R12.2>.
20. ASTM: American Society for Testing and Materials. ASTM D882: standard test method for tensile properties of thin plastic sheeting. West Conshohocken: ASTM; 2018. <http://dx.doi.org/10.1520/D0882-18>.
21. Li G, Tian X, Xu X, Zhou C, Wu J, Li Q, et al. Fabrication of robust and highly thermally conductive nanofibrillated cellulose/graphite nanoplatelets composite papers. *Compos Sci Technol*. 2017;138:179-85. <http://dx.doi.org/10.1016/j.compscitech.2016.12.001>.